JOURNAL OF PROPULSION AND POWER
Vol. 14, No. 3, May–June 1998

Study on Trapped-Vortex Combustor—Effect of Injection on Flow Dynamics

Viswanath R. Katta*
Innovative Scientific Solutions, Inc., Dayton, Ohio 45440-3638
and
W. M. Roquemore†
U.S. Air Force Research Laboratory, Wright–Patterson Air Force Base, Ohio 45433-7103

Low-velocity flows in the cavities of a combustor can aid in establishing stable flames. However, unsteady flows in and around cavities may destabilize these flames. By proper cavity design it is possible to lock (trap) the vortices spatially and, thereby, stabilize the flames. The spatially locked vortices restrict the entrainment of main air into the cavity. For obtaining good performance characteristics with a trapped-vortex combustor, a sufficient amount of fuel and air must be injected directly into the cavity. This mass injection can alter the dynamic characteristics of the flow inside and around the cavity. The present study employed a numerical simulation to investigate the vortex dynamics of a cavity into which fluid mass is directly injected through jets. A third-order-accurate, time-dependent, computational fluid dynamics with chemistry code was used for simulating the dynamic flows associated with an axisymmetric, centerbody trapped-vortex combustor under nonreacting and reacting conditions. It was found that mass injection increases the optimum size (width-to-diameter ratio) of the cavity. Injection of small amounts of fluid into a nonoptimum cavity increases the unsteadiness of the flow. Fluid injected into the optimum-size cavity is transported along the outer core of the vortex, providing more efficient mixing and a longer residence time for the fuel/air mixture. It was also found that use of thinner afterbodies results in the cavity flow being more dynamic. Calculations made with a global-chemistry model revealed that at higher annulus air velocities, combustion is limited to the cavity region. As in the case of cold flows, the injection jets in reacting flows are pushed outward from the center when the cavity size is small.

Nomenclature

A = coefficient used in finite difference equation
C_p = pressure coefficient
c_p = specific heat of the mixture
D = diffusion coefficient
D_0 = forebody diameter
dA = incremental area
H = enthalpy
h = total enthalpy
h_f^0 = heat of formation at standard state
Le = Lewis number
M = molecular weight
N_s = total number of species
p = pressure
R_0 = universal gas constant
r = radial distance
S_n = number of wall surfaces
S^Φ = source term in Φ equation
T = temperature
t = time
u = axial velocity component
V = velocity
v = radial velocity component
X_c = cavity length
Y = mass fraction
z = axial distance
Γ^Φ = transport coefficient in Φ equation
ΔH = disk thickness
λ = thermal conductivity
μ = viscosity
ρ = density
Φ = represents a flow variable
$\dot{\omega}$ = net rate of production of a species

Subscripts
i = ith species
j = jth reaction
P = reference grid point
w = wall
z^+, r^+ = grid points adjacent to P in z and r directions, respectively
z^{++}, r^{++} = two grid points away from P in z and r directions, respectively
z^-, r^- = grid points adjacent to P in negative z and r directions, respectively
z^{--}, r^{--} = two grid points away from P in negative z and r directions, respectively
∞ = freestream

Superscript
N = time-step number

Presented as Paper 97-3256 at the AIAA/ASME/SAE/ASEE 33rd Joint Propulsion Conference and Exhibit, Seattle, WA, July 6–9, 1997; received Aug. 25, 1997; revision received Jan. 30, 1998; accepted for publication Jan. 30, 1998.

*Senior Engineer, 2786 Indian Ripple Road.
†Senior Scientist, Propulsion Directorate.

Introduction

UNSTEADY flow in and around cavity-type geometries occurs in a variety of applications such as slotted wind tunnels, slotted flumes, bellow-type configurations, and aircraft engine and airframe components. In particular, the unsteady flow in aircraft combustors limits fuel-lean operation and degrades flame-stability characteristics. Recently, a simple, compact, and efficient method of using cavities to stabilize combustion was proposed by Hsu et al.[1] Because this concept uses

a vortex that is trapped in a cavity to stabilize the flame, it is referred as the trapped-vortex (TV) concept. Several investigators have recognized the aerodynamic advantages of locking the vortices inside and around the cavity in a nonreacting flow.[2–4] Experiments of Rohsenow et al.[2] have shown that when two circular orifices are placed in series in a pipe, a large recovery of pressure occurs across the second orifice in certain circumstances; hence, the overall pressure drop is considerably less for the two orifices than for a single one having the same flow. In ribbed diffusers, Migay[3] found that balancing the fluid removed by entrainment and the fluid entering the cavity by reversed flow ensures that the flow outside the cavities will follow the ribs fairly closely, and a good pressure recovery will be achieved. Mair[4] showed that by mounting a disk behind the base of a blunt body, the drag of the blunt object can be reduced. Using similar concepts, Roshko and Koenig[5] reported a reduction in drag of blunt forebodies when disks were placed on spindles ahead of the bodies.

Little and Whipkey[6] conducted extensive investigations on the dynamic nature of flows over bluff bodies using smoke-flow visualization and laser–velocimetry (LV) techniques. Because of the limitations of the smoke tunnel, they employed reduced-flow conditions (~0.3 m/s) and half-scale geometries for the flow-visualization studies and full-scale geometries and turbulent flows (~30 m/s) for the time-averaged drag measurements. Based on these reduced and full-scale experiments, they correlated the afterbody drag and the motion of the vortex in the wake region and postulated that a minimum-drag condition is established when the wake vortices are locked between two disks mounted in series on a spindle. They also suggested that the cavity formed between the disk and the bluff body should be of such dimensions that the locked vortex would effectively fill the cavity. Based on reduced-scale, flow-visualization experiments on cavities formed between a forebody and an afterbody, Little and Whipkey correlated the drag and motion of the vortex in the cavity region and postulated that a minimum-drag condition is established when the cavity vortices are locked between the two bodies. Katta and Roquemore[7,8] used direct numerical simulations to investigate the Little and Whipkey experiments under turbulent-flow conditions. The simulations successfully predicted that a cavity having a length-to-diameter ratio of 0.45 becomes stationary and that the pressure-drag coefficient is reduced to a minimum value when the vortices are locked inside and around the cavity. This suggests that the relationship between the minimum drag coefficient and the vortex motion is also valid in the case of turbulent flows. These simulations demonstrated the capability of numerical simulations in the study of the dynamic processes associated with cavities.

Two major differences exist between flows associated with airframe cavities and those associated with the combustor cavities. First, the heat release and higher viscosity of the combustion products associated with the partial burning that takes place in the cavities could alter the vortex dynamics. As a result, the criterion for trapping a vortex in a heated flow would differ from that for trapping a vortex in a cold flow. Secondly, it is known that a locked vortex entrains a minimum amount of fluid from the main flow; hence, to achieve continuous combustion in trapped-vortex combustors, fuel and air must be directly fed into the cavity. Experimental investigations of Hsu et al.[1] also indicate that a TV combustor operates most efficiently when fuel and air are injected directly into the cavity. However, direct injection of mass (air and/or fuel) into the cavity could alter the geometrical criterion derived for locking vortices inside passive cavities, i.e., without injection.

The purpose of this study was to investigate the dynamics of cavity flows as jets are directly injected into the cavity. A third-order-accurate, time-dependent, computational fluid dynamics with chemistry (CFDC) code and a large number of grid points were used to investigate the flowfields in a research TV combustor[1] under nonreacting and reacting flow conditions.

Modeling

A time-dependent, axisymmetric mathematical model that solves for axial- and radial-momentum, continuity, and enthalpy- and species-conservation equations is used to simulate the flowfields in the TV combustor. The governing equations, written in a cylindrical-coordinate system, are as follows:

$$\frac{\partial \rho}{\partial t} + \frac{\partial \rho u}{\partial z} + \frac{1}{r}\frac{\partial (r\rho v)}{\partial r} = 0 \tag{1}$$

$$\frac{\partial (\rho\Phi)}{\partial t} + \frac{\partial (\rho u\Phi)}{\partial z} + \frac{1}{r}\frac{\partial (r\rho v\Phi)}{\partial r} = \frac{\partial}{\partial z}\left[\Gamma^{\Phi}\frac{\partial \Phi}{\partial z}\right] + \frac{\partial}{\partial r}\left[r\Gamma^{\Phi}\frac{\partial \Phi}{\partial r}\right] + S^{\Phi} \tag{2}$$

Here u and v are the axial and radial components of the velocity vector, respectively. The general form of Eq. (2) represents the momentum, the species, or the energy-conservation equation, depending on the variable used in place of Φ. In Table 1 the transport coefficients Γ^{Φ} and the source terms S^{Φ} that appear in the governing equations are given.

The partial set of equations represented by Eqs. (1) and (2) can be completed using the global-species-conservation equation

$$Y_{N_s} = 1.0 - \sum_{i}^{N_s - 1} Y_i \tag{3}$$

and the state equation

$$p = \rho T R_0 \sum_{1}^{N_s} \left(\frac{Y_i}{M_i}\right) \tag{4}$$

where Y_i and M_i are the mass fraction and molecular weight of the ith species, respectively. While density is obtained by solving the state equation [Eq. (4)], the pressure field at every

Table 1 Transport coefficients and source terms in governing equations

Φ	Γ^{Φ}	S^{Φ}
u	μ	$\frac{\partial p}{\partial z} + \frac{\partial}{\partial z}\left(\mu\frac{\partial u}{\partial z}\right) + \frac{\partial}{\partial r}\left(\mu\frac{\partial v}{\partial z}\right) + \frac{\mu}{r}\frac{\partial v}{\partial z} - \frac{2}{3}\left\{\frac{\partial}{\partial z}\left(\mu\frac{\partial u}{\partial z}\right) + \frac{\partial}{\partial z}\left(\mu\frac{\partial v}{\partial r}\right)\right\} + \frac{\partial}{\partial z}\left(\mu\frac{v}{r}\right)$
v	μ	$\frac{\partial p}{\partial r} + \frac{\partial}{\partial z}\left(\mu\frac{\partial u}{\partial r}\right) + \frac{\partial}{\partial r}\left(\mu\frac{\partial v}{\partial r}\right) + \frac{\mu}{r}\frac{\partial v}{\partial r} - 2\mu\frac{v}{r^2} - \frac{2}{3}\left\{\frac{\partial}{\partial r}\left(\mu\frac{\partial u}{\partial z}\right) + \frac{\partial}{\partial r}\left(\mu\frac{\partial v}{\partial r}\right)\right\} + \frac{\partial}{\partial r}\left(\mu\frac{v}{r}\right)$
H	λ/c_P	$\nabla\left[\frac{\lambda}{c_P}\sum_{1}^{N}\{(Le^{-1}-1)H_i\nabla Y_i\}\right] - \sum_{1}^{N}(h_{f_i}^{o}\dot{\omega}_i)$
Y ($i = 1 \sim N_s - 1$)	ρD_{i-N_2}	$\dot{\omega}_i$

time step is determined from pressure Poisson equations. Even though governing equations are solved in an uncoupled manner, species-conservation equations are coupled through the source terms during the solution process to improve the stability of the algorithm. Temperature- and species-dependent thermodynamic and transport properties are used in this formulation. The enthalpy of each species is calculated from polynomial curve fits; the viscosity, thermal conductivity, and diffusion coefficients of the species are estimated from the Lennard–Jones potentials.

In the present work reacting flows were simulated using the following global-chemical-kinetics model involving propane, oxygen, water, carbon dioxide, and nitrogen:

$$C_3H_8 + 5O_2 + 17.73N_2 \Rightarrow 3CO_2 + 4H_2O + 17.73N_2 \quad (5)$$

The specific reaction rate for Eq. (5) is written in Arrhenius form with a very large pre-exponential factor.

The governing equations are integrated using an implicit QUICKEST (quadratic upstream interpolation for convective kinematics with estimated streaming terms) numerical scheme,[9,10] which is third-order accurate in both space and time and has a very low numerical-diffusion error. An orthogonal, staggered-grid system with rapidly expanding cell sizes in both the z and r directions is utilized for discretizing the governing equations. After rearrangement of terms, the finite difference form of the governing equation for the variable Φ at a grid point P can be written as an algebraic equation as follows:

$$A_P\Phi_P^{N+1} + A_{z^{++}}\Phi_{z^{++}}^{N+1} + A_{z^{+}}\Phi_{z^{+}}^{N+1} + A_{z^{-}}\Phi_{z^{-}}^{N+1} + A_{z^{--}}\Phi_{z^{--}}^{N+1} + A_{r^{++}}\Phi_{r^{++}}^{N+1} + A_{r^{+}}\Phi_{r^{+}}^{N+1} + A_{r^{-}}\Phi_{r^{-}}^{N+1} + A_{r^{--}}\Phi_{r^{--}}^{N+1} = S_P^{\Phi} + \Delta t \cdot \rho_P \Phi_P^{N} \quad (6)$$

The time increment t is determined from the stability constraint and maintained as a constant during the entire calculation. The superscripts N and $N + 1$ represent the known variables at the Nth time step and the unknown variables at the $(N + 1)$th time step, respectively; the subscripts z^+ and z^- indicate the values at the grid points immediately adjacent to point P in the positive and negative z directions, respectively. Similarly, the subscripts z^{++} and z^{--} represent the values at two grid points from P in the respective directions. The coefficients A and the terms on the right-hand side of the previous equation are calculated from the known flow variables at the Nth time step. The preceding equations for $N_s + 2$ variables are solved individually using an iterative alternative direction implicit technique. The pressure field at every time step is accurately calculated by simultaneously solving the system of algebraic pressure Poisson equations at all grid points using the lower–upper (LU) decomposition technique.

Flat-velocity profiles are used at the main and primary inflow boundaries. A simple extrapolation procedure[11] with weighted zero- and first-order terms is employed to estimate the flow variables at the outflow boundary. The usual no-slip, adiabatic, and chemically inert boundary conditions are applied at the walls.

Model Validation

The CFDC code developed on the basis of the methodology described in the previous section was used previously to investigate various dynamic flows in both reacting and nonreacting environments. In conjunction with global-chemistry[10] and finite rate chemistry[12] models, the code was successfully used to predict the dynamic characteristics of jet diffusion and premixed flames. After incorporation of a finite rate global chemistry model, it was also used to investigate the attached and lifted flames in a swirl-stabilized step combustor,[13] and a reasonable correlation between experimental results and calculations was obtained.

Nonreacting flow calculations for geometries similar to the one employed in the present investigation showed that the vortex shedding behind a bluff body can lead to a higher drag coefficient.[7] Those simulations also demonstrated that by proper choice of cavity size, the vortices within the cavity and behind the afterbody can be locked and, thereby, the drag coefficient of the forebody–spindle–disk combination decreased. For different cavity sizes the predicted dynamics of the vortices formed inside the cavity and behind the forebody compared well with the results of smoke visualizations and LV measurements of Little and Whipkey.[6]

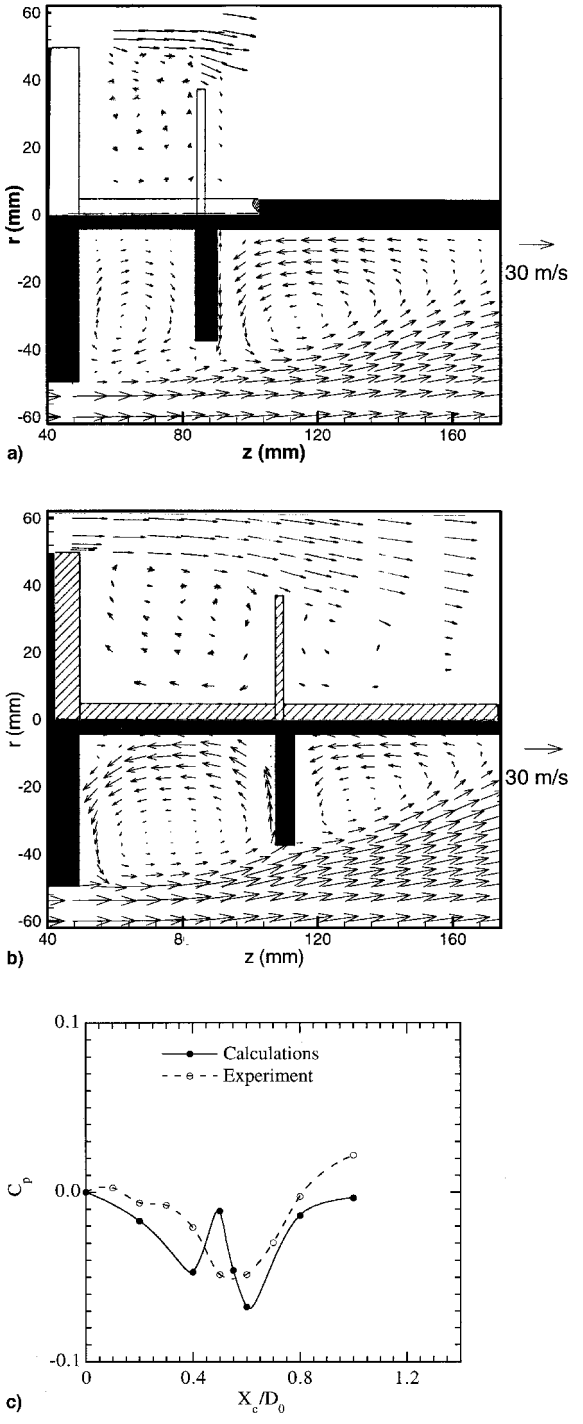

Fig. 1 Computed and measured velocity fields around forebody–spindle–disk geometry for a) smaller-than-optimum and b) optimum size cavities. c) Change in pressure coefficient for different cavity sizes. Experimental data are taken from Ref. 6.

Typical results obtained for the forebody–spindle–disk geometry of Little and Whipkey are shown in Fig. 1 along with the corresponding experimental data. An annular air velocity of 30 m/s was used in both the calculations and the experiment. As discussed previously, flow within the cavity and behind the disk became dynamic for cavity sizes other than the optimum one. The flowfield obtained for a smaller-than-optimum ($X_c/D_0 = 0.35$) size cavity is shown in Fig. 1a, and that for the optimum ($X_c/D_0 = 0.6$) one is shown in Fig. 1b. Here, the computed velocities (shown in the lower half) are obtained by time-averaging over 8000 instantaneous solutions, and the measured velocities (upper half) represent the time-averaged LV data. Figures 1a and 1b suggest that calculations have captured the key features of these dynamic flows; namely, a steady flow in the optimum-size cavity, an unsteady flow in the smaller-than-optimum size cavity, multiple-vortex structure within the cavities, and the direction of rotation of the vortices. Note that in the smaller-than-optimum size cavity, the larger vortex is rotating in the direction opposite that in the optimum-size cavity. Interestingly, time-averaged calculations using the k-ε model failed to predict these features. Details of these calculations were given in Ref. 7.

Changes in the pressure drag coefficient resulting from the addition of different size cavities to the forebody are shown in Fig. 1c. Both the calculations and the experimental results indicate that the drag coefficient becomes minimum for $X_c/D_0 \sim 0.6$. In addition, calculations predicted a sudden increase in the drag coefficient for $X_c/D_0 \sim 0.5$. Even though the experimental data did not show such a spike in the drag-coefficient curve, additional measurements[6] made with a slightly thicker spindle yielded similar spikes. Overall, the dynamic calculations performed on forebody-spindle-disk geometries using the CFDC code described earlier have yielded satisfactory results. The grid spacing of ~0.9 mm in the z and r directions used in these simulations was found to be sufficient to capture the large-scale structures whose physical size is greater than the length scales that are an order of magnitude smaller than the cavity height. Because the code and the calculation methodology adopted in the present investigations of injection effects on cavity flows are essentially the same as those used for the forebody-spindle-disk cases, the accuracy of the results presented in this paper is expected to be comparable to that obtained in the earlier work.[7] In addition, a grid spacing of ~0.5 mm (nearly half of that used in the previous studies on locked vortices) in the z and r directions was used in the present simulations primarily to resolve the injection jets.

Results and Discussion

The geometry chosen for the present study is similar to that of the TV combustor designed by Hsu et al.,[1] and to that used by Little and Whipkey[6] in their cold-flow experimental investigations on locked vortices. It consists of a 70-mm-diam flat cylindrical forebody enclosed in an annular cylindrical tube having an 80-mm i.d. An afterbody disk having a diameter and thickness of 50.8 and 20 mm, respectively, is attached to the forebody using a 9-mm-diam centerbody. The size of the cavity formed between the forebody and the afterbody is varied by moving the latter toward or away from the former. Airflow over this body develops vortices inside the cavity and behind the afterbody; normally these vortices shed, and the flow becomes dynamic in nature. The velocity of the air used in the annular gap between the forebody and the surrounding tube is 40 m/s. Primary air and fuel (propane) are injected into the cavity from the afterbody. Fuel and air are carried to the afterbody through a central tube that connects the afterbody to the forebody. The geometry and the grid system used are shown in Fig. 2. Variation of the grid spacing was adopted in both the axial z and radial r directions to cluster the grid points in the cavity and near the walls.

In the experiments of Hsu et al.,[1] fuel and air were introduced into the cavity from concentric holes on the afterbody. However, in the present axisymmetric simulations, these injection holes are grouped into three annular ring jets with the fuel jet sandwiched between the airjets. Based on the hole size and mean distance from the centerline, the reconstructed annular jets of 1-mm thickness are located in the afterbody, as shown in Fig. 2. The centers of these three annular jets (A, B, and C) are located 11, 14, and 19 mm from the axis of symmetry, respectively. Jets A and C represent air, and jet B represents fuel (propane) in the experiment and in the combusting-flow calculations; however, for simplification, all three jets are assumed to be airjets in the nonreacting calculations. Exit velocities for jets A, B, and C are 12.4, 5.0, and 12.4 m/s, respectively. This fuel and air injection results in a global (or overall) equivalence ratio of 0.2 in the combustor and a primary equivalence ratio (defined as the fuel-to-air ratio injected

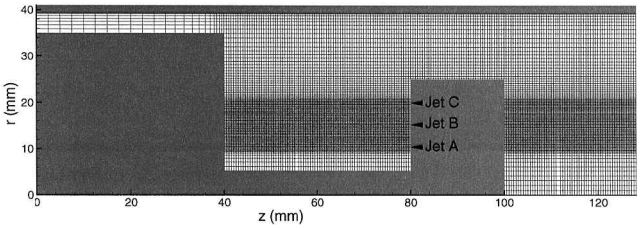

Fig. 2 Geometry and grid system used for studying effects of injection on dynamic characteristics of flows in cavity formed between the forebody and afterbody of an axisymmetric trapped-vortex combustor.

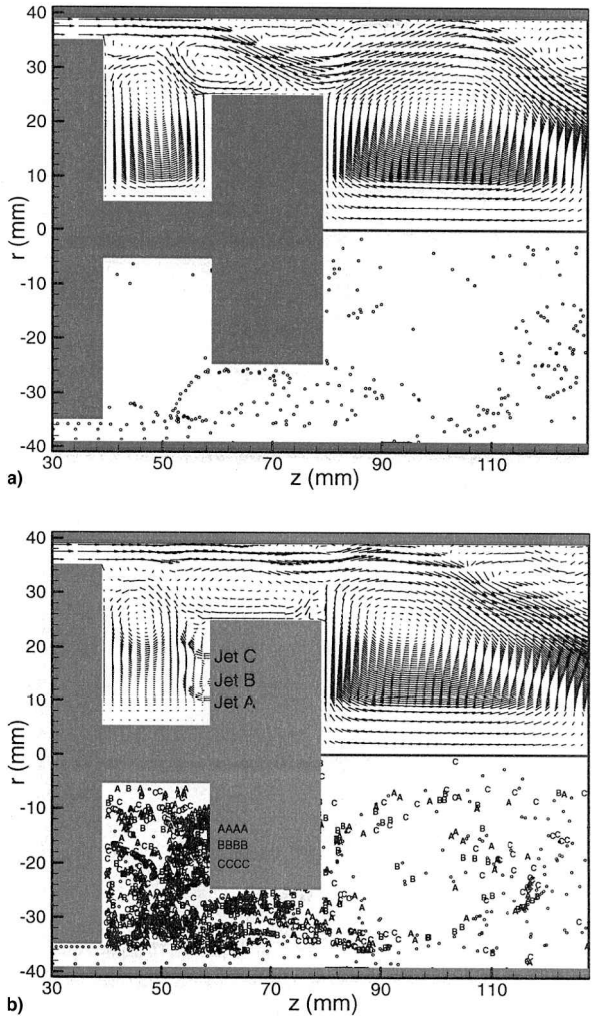

Fig. 3 Instantaneous nonreacting flowfields obtained for small-size cavity a) without and b) with cavity injection.

into the cavity relative to the ratio required for stoichiometric combustion) of 4.4 in the cavity.

Starting from a uniform initial flowfield in the combustor, direct numerical simulations are made for different cavity sizes and injection conditions. For obtaining results not biased by the initial uniform flowfield, initial calculations for 25,000 time steps (corresponding to 0.600 s of real time) were discarded prior to recording the dynamic solutions. Calculations were then continued for another 5000 time steps for data-analysis purposes.

For understanding the influence of fluid injection on flow dynamics, calculations were made for different injection conditions and afterbody locations. A 341 × 101 grid system was used in the calculations. Instantaneous flowfields obtained for three cavity sizes are shown in Figs. 3, 4, and 5. Hsu et al.[1] found that the cavity size given in Fig. 4 yielded optimum performance under combustion conditions. The width-to-diameter (forebody) ratio of this cavity is 0.57. The smaller and larger cavities shown in Figs. 3 and 5 have width-to-diameter ratios of 0.285 and 0.855, respectively. The flowfields obtained for small-, medium-, and large-size cavities with cavity injection are shown in Figs. 3b, 4b, and 5b, respectively. In these figures instantaneous velocity fields are shown on one side of the combustor, and traces of the particles injected from different locations are shown on the other side.

Passive Flows in Cavity

It is known that passive-cavity flows (without injection or combustion) become unsteady for cavity sizes that are smaller

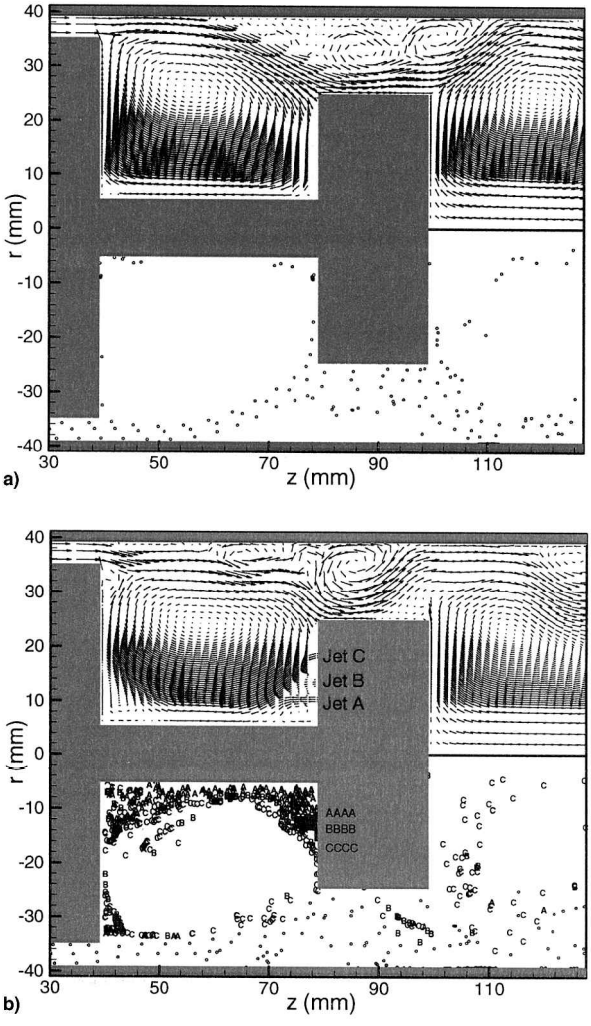

Fig. 4 Instantaneous nonreacting flowfields obtained for medium (optimum)-size cavity a) without and b) with cavity injection.

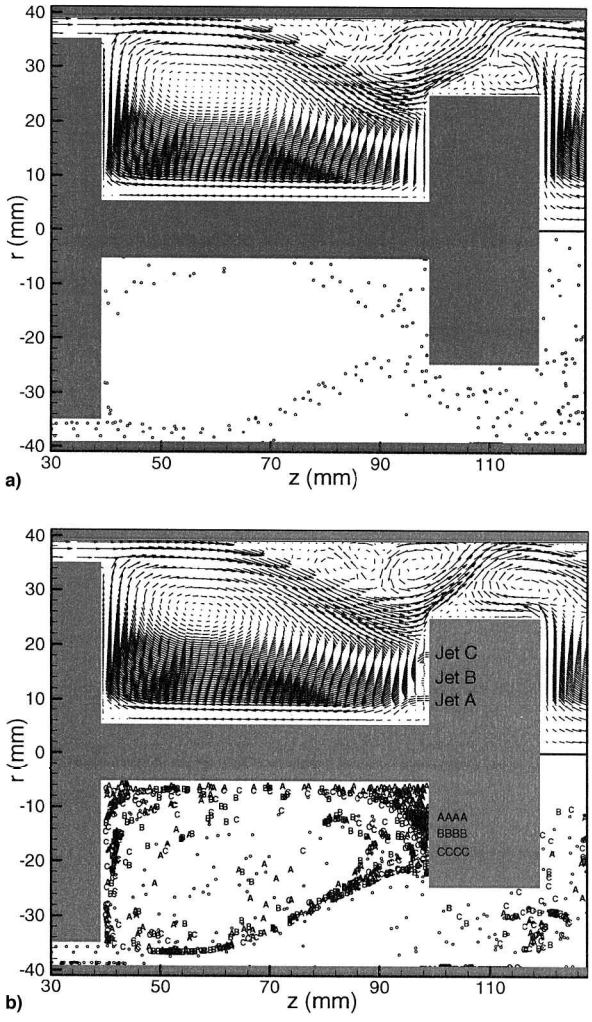

Fig. 5 Instantaneous nonreacting flowfields obtained for large-size cavity a) without and b) with cavity injection.

or larger than the optimum. Instantaneous results obtained for the smaller-size cavity (Fig. 3a) indicate that the flowfield is quite complex as a result of the formation of several vortices. Because of the presence of the cavity, the main flow is expanded toward the centerbody which, in turn, results in flow separation on the outer wall. Interestingly, fluid in the cavity is rotating counterclockwise and is separated from the main flow by two other vortices that are rotating naturally in the clockwise direction. Several instantaneous solutions of this flow revealed that the vortices in the cavity are not shedding but moving back and forth within the cavity. This is expected because the expanding main flow confines the cavity vortices by impinging on the thick afterbody (20 mm). Further calculations made with a thinner afterbody resulted in significant vortex shedding from the cavity. Because of the lack of vortex shedding from the cavity, only a few particles that are injected into the main flow enter the cavity. However, the widely distributed particles behind the afterbody suggest that the flow is quite dynamic.

For the medium- and large-size cavities, only one major vortex is formed within the cavity. The flow is unsteady because this vortex is moving inside the cavity. The particle traces suggest that the flow around the large-size cavity (Fig. 5a) is more dynamic than that around the medium-size cavity (Fig. 4a). In the latter case, the main flow is expanding and entering the cavity slightly upstream of the forebody. The particles injected into the main flow are directly entering the cavity. This means that the size (width) of the cavity might be larger than the optimum size for trapping the vortices. This cavity size was

determined experimentally to be optimum in a combustion environment. However, it may not represent the optimum size for a nonreacting flow environment. The major differences between cold and combusting flows from a cavity-flow dynamics viewpoint are 1) the damping effect of heat release on flow instabilities, and 2) the addition of mass into the cavity from primary-fuel and air injections.

Effect of Injection on Cold Flows in a Cavity

For understanding the mass-addition effects of jets on cavity-flow dynamics, calculations were made with air injections for the cavity sizes shown in Figs. 3a, 4a, and 5a; the resulting instantaneous flowfields are plotted in Figs. 3b, 4b, and 5b, respectively. The convective transport of the injected fluids is visualized by representing the particles that are released from jets A, B, and C by symbols A, B, and C, respectively. Note that the particles released from the main flow are represented by open circles.

The addition of mass into the cavity increased the unsteadiness of the flow in the cases of small- and large-size cavities (Figs. 3b and 5b, respectively). This is evident from the increase in the number of main-flow particles (open circles) in the cavity. Very few main-flow particles enter the medium-size cavity (Fig. 4b) when injection is introduced. This suggests that mass addition has a stabilizing effect on the flow in the medium-size cavity and a destabilizing effect in the other two cases. The particle trajectories also reveal that the mass injected from the three jets is distributed more in the small- and large-size cavities than in the medium-size one. In fact, the three jets are confined to the outer core of the trapped vortex (Fig. 4b), and only particles released from jet C are entrained into the wake behind the afterbody. Based on these calculations, one might intuitively predict the scenario for the combusting cases. For an overall equivalence ratio of 0.2, the increased mixing between the primary jets and the cavity flow in the nonoptimum cavities could locally make the mixture fuel-lean. When the cavity becomes unsteady, one might expect significant intermittent burning, which, in turn, leads to poor combustion efficiency. In the medium-size-cavity case, all three jets are transported stably around the cavity vortex, which enhances the mixing of jets. As the fuel and air are injected at a primary equivalence ratio of 4.4, the mixture is

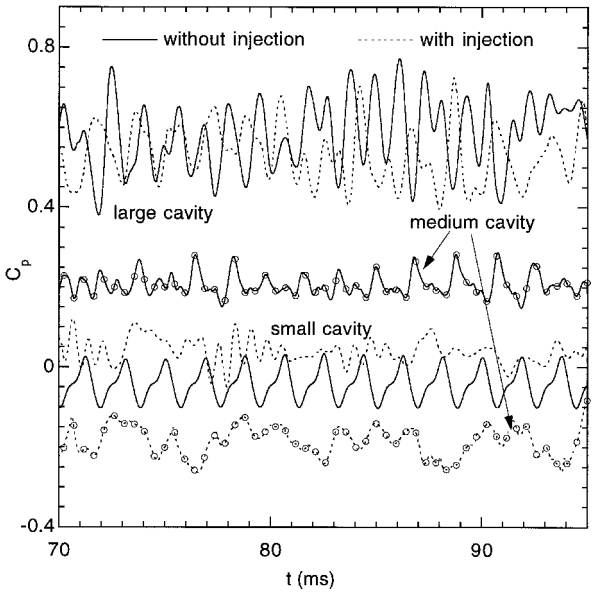

Fig. 6 Variation of pressure coefficient for different cavity sizes without and with injection.

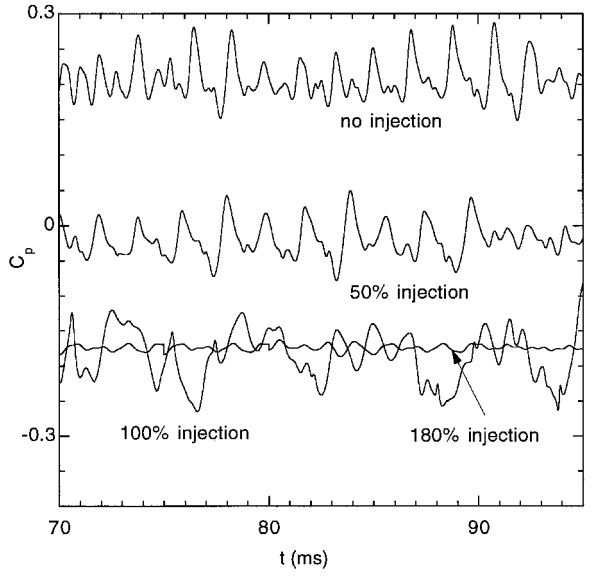

Fig. 7 Effect of injection mass on pressure coefficient.

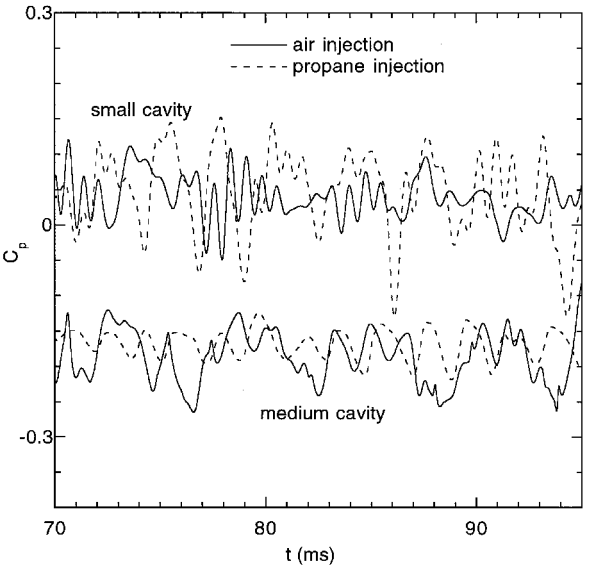

Fig. 8 Comparison of pressure coefficients predicted with air and propane injections for two different cavity sizes.

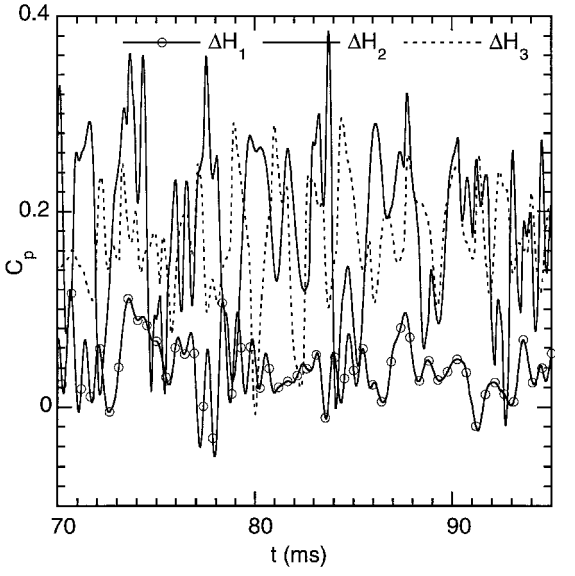

Fig. 9 Effect of afterbody thickness on pressure coefficient. H_1, H_2, and H_3 represent 20-, 10-, and 5-mm thicknesses, respectively.

expected to burn steadily in the outer core of the cavity vortex, and combustion would occur at the maximum extent, depending on the physical dimensions of the cavity or the residence time. The experiments of Hsu et al.[1] clearly demonstrated these features of the TV combustor. They obtained stable and intense burning when fuel and air were injected into the medium-sized cavity at a primary equivalence ratio of 4.4.

Flow unsteadiness in combustors not only causes the flames to burn inefficiently but also increases the pressure force across the combustor. The pressure coefficient C_p is calculated using the expression

$$Cp = \sum_{1}^{Sn} \frac{1}{\rho_\infty V_\infty^2} \int (p_w - p_\infty)\, dA \qquad (7)$$

Here, p_w and p correspond to wall and freestream pressures, respectively, and S_n represents the number of wall surfaces in the computational domain. The calculated C_p as a function of time is shown in Fig. 6 for the six cases discussed earlier. The solid curves of this figure represent the pressure coefficient in the absence of cavity injection. It should be noted from the plot that the small cavity has the lowest C_p. However, when injection is included, the pressure coefficient of the small cavity increases slightly, remains at the same higher level for the large cavity, and decreases significantly in the medium-size cavity. In fact, the medium cavity with injection has the lowest pressure coefficient among the six cases considered.

Even though the medium-size cavity with injection yielded the lowest C_p, it still does not exhibit a perfectly steady flow pattern. This could be caused by either insufficient or excess mass injection into the cavity. For understanding the effect of mass injection on flow dynamics, two additional calculations were made for the medium-size cavity with injections of 50 and 180% of the mass used in the calculations shown in Fig. 6. The pressure coefficients for different injection cases are plotted in Fig. 7. These calculations suggest that 1) the frequency of the oscillations decreases with injection mass, 2) the pressure coefficient for 180% injection becomes nearly steady, and 3) the pressure coefficient decreases with injection mass.

Figure 8 shows the differences in pressure-coefficient fluctuations with air and propane injections. Here, the middle jet (jet B) is replaced with propane fuel, and injection mass is the

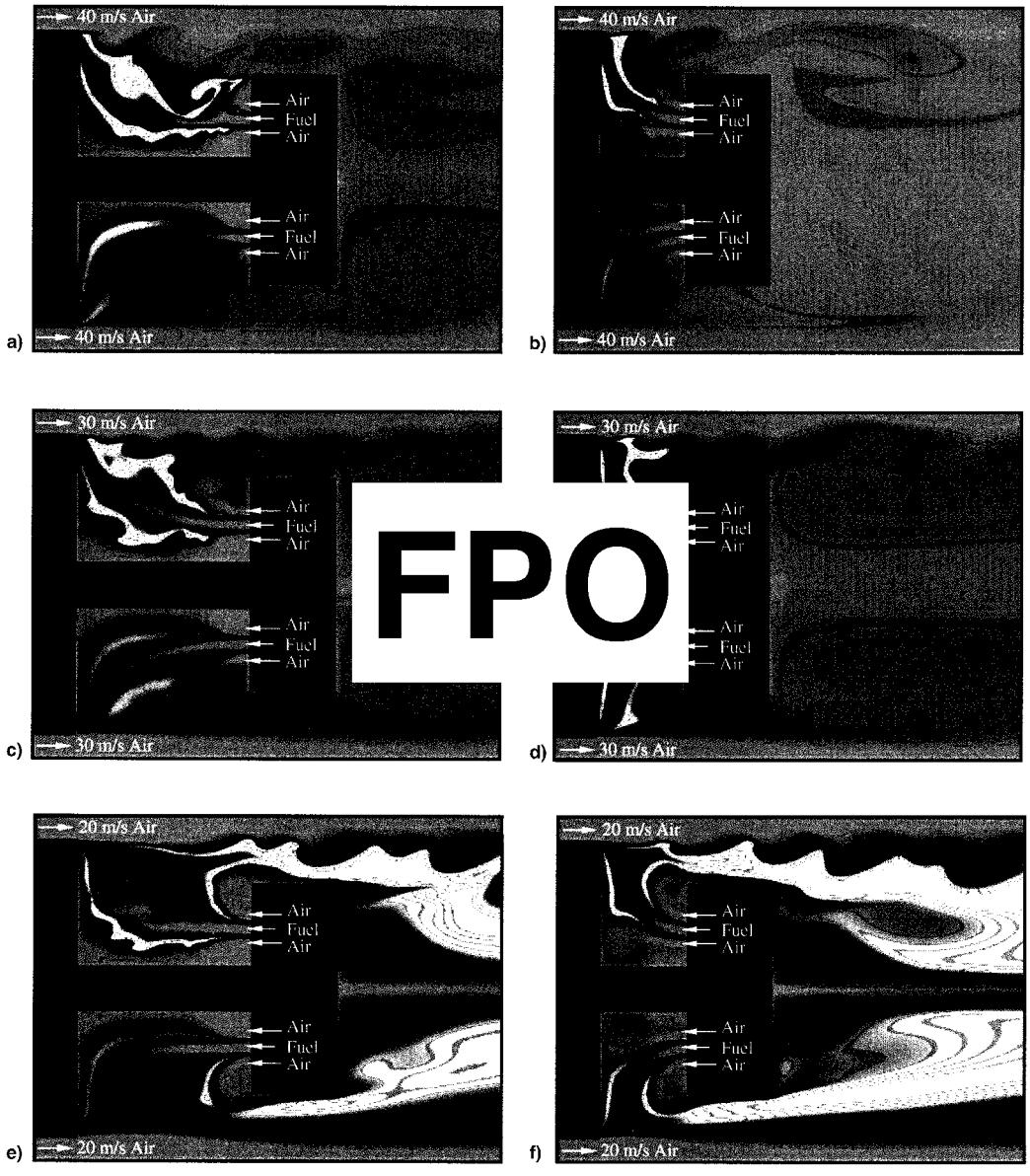

Fig. 10 Reacting flowfields obtained for different main-flow velocities. In each plot temperature variation between 300 K (blue) and 2000 K (red) is shown with rainbow color palette. Instantaneous and time-averaged data are shown in upper and lower halves, respectively. a) Medium- and b) small-size cavity flows for a main-flow velocity of 40 m/s. c) Medium- and d) small-size cavity flows for a main-flow velocity of 30 m/s. e) Medium- and f) small-size cavity flows for a main-flow velocity of 20 m/s.

same as that in Fig. 6. The density variation appears to have no impact on the medium-size cavity; in the small-size-cavity case, however, propane injection generates slightly higher amplitude pressure fluctuations. The effect of afterbody thickness on the unsteady flow inside and around the cavity was studied by simulating the flow over three afterbody thicknesses. These calculations were performed for the small-size cavity with normal (100%) air injection. Fluctuating pressure coefficients as functions of time are plotted in Fig. 9. While H_1 represents the thickness of the standard afterbody (20 mm), H_2 and H_3 represent 50 and 25% of the thickness of the standard afterbody, respectively. As expected, the thinner afterbodies provided better communication between the cavity and the afterbody-wake flows. This resulted in increased pressure coefficients. The larger-amplitude fluctuations for the thinner afterbodies suggest increased vortex shedding from the cavity.

Effect of Combustion on Cavity Flows

For investigating the vortex characteristics in the cavity under combusting-flow conditions, calculations were made for the simulation of reacting flow in the combustor described previously. Hsu et al.[1] found that this combustor operates most stably when the cavity size is at the optimum value (Fig. 4) and when the primary air and fuel (propane) are injected into the cavity at an equivalence ratio of 4.4. Calculations were made for this fuel-rich condition using the 341 × 101 grid system.

The instantaneous and time-averaged temperature fields computed with a fast-chemistry assumption are shown in the upper and lower halves of Fig. 10a, respectively. In general, the center fuel jet is mixing with the neighboring airjets and burning as two distinct flames. The instantaneous-temperature field suggests that the flow in the cavity has a large vortex generated by the high-speed annulus airflow and several small vortices that have developed primarily from the interaction of fuel and air jets injected into the cavity. Small puffs of fuel are penetrating through the outer airjet periodically. The existence of jet-like flame structures in the time-averaged temperature field in Fig. 10a indicates that the large cavity vortex is nearly stable. Note that for this cavity size, cold-flow calculations with injection also yielded a nearly stable vortex within the cavity (Fig. 4b).

The effect of cavity size on combustion was studied by simulating the reacting flow in a 50% smaller cavity and by maintaining the same injection velocities for the fuel and airjets as those used for the optimum-size-cavity calculations. The instantaneous and time-averaged temperature fields are shown in Fig. 10b. Interestingly, the combustion is still confined within the cavity, even though the lengths of the jet-like flames have been reduced by nearly one-half. A significant amount of fuel is escaping from the cavity, mixing with the annulus air, and burning without raising the local temperature significantly as the mixture becomes very fuel-lean. As the cavity vortex becomes weaker in the case of the smaller-size cavity (Fig. 10b), the flames are pushed away from the center tube. This behavior is also seen in the cold-flow simulations made with injection (Figs. 3b).

Reacting-flow calculations were also made for different annulus-airflow velocities on the optimum-size and smaller-size cavities. Results obtained for a 30-m/s annulus flow are shown in Figs. 10c and 10d for the two cavity sizes, and those obtained for a 20-m/s annulus flow are shown in Figs. 10e and 10f. As expected, the strength of the cavity vortex is decreasing with reduction in annulus airflow. Because of this the outer airjet is turning back around the afterbody and the separation between the two flame jets has increased. The lower annulus airflow is also increasing the local equivalence ratio outside the cavity which, in turn, results in higher temperatures downstream of the afterbody. This behavior was also experimentally observed by Hsu et al.[1] In addition, for lower annulus flows, the shear-layer vortices are becoming more organized.

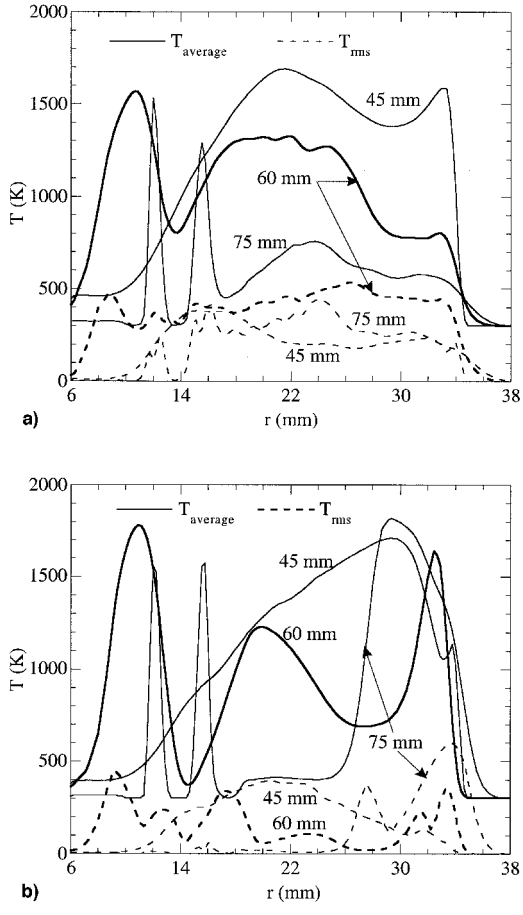

Fig. 11 Radial distributions of mean and rms temperature at different axial locations in the cavity for annular air velocities of a) 40 and b) 20 m/s.

For quantifying the unsteadiness associated with the combusting flows shown in Fig. 10, the mean and rms temperatures are obtained from 20,000 instantaneous solutions over a period of 120 ms. Figures 11a and 11b show the radial distributions of these temperatures at different axial locations in the medium-sized cavity operating at annular-air velocities of 40 and 20 m/s, respectively. The three axial distances in the cavity z = 45, 60, and 75 mm correspond to locations 1) near the forebody, 2) at the center of the cavity, and 3) near the disk, respectively. As expected, the rms temperatures in the 20-m/s case are smaller than those obtained with the 40-m/s air velocity. Overall, the low level of rms (<500 K) values for the temperature fluctuations noted in the cavity region is very similar to that observed in the experiments.[1]

Summary and Conclusions

Unsteady flow inside and around the cavity, in general, leads to a higher drag coefficient, and in combustors it creates further problems related to blowout and poor combustion efficiency. It is known that the unsteadiness of the flow can be reduced by proper cavity design. The dynamics of the vortices formed inside and around the cavity was studied using a time-dependent, axisymmetric CFDC code. The geometry used in this study was an axisymmetric, centerbody trapped-vortex combustor employed by Hsu et al.[1] A large number of grid points with z and $r \sim 0.5$ mm was used to capture the vortical structures having length scales that are an order of magnitude smaller than the height of the cavity. Fluid was injected into the cavity from three locations at different flow rates to investigate the effects of fluid injection on vortex dynamics. It was found that the optimum cavity size for obtaining steady flow inside and around the cavity should be larger in the case of

fluid injection than for passive cavities (with no injection). The flow becomes more unsteady when the fluid is injected into nonoptimum (larger or smaller than the optimum) cavities. Calculations made with air and propane injections yielded very similar flow patterns and pressure coefficients. On the other hand, the thickness of the afterbody seems to have a strong influence on the flow pattern. Thinner afterbodies resulted in higher pressure coefficients, with fluctuations larger than those observed with the thicker afterbodies.

Calculations made using a single-step global-chemistry model revealed that the fuel injected into the cavity mixes with the injected air and burns like a jet flame. It was found that a lesser amount of fuel is burned in the smaller-size cavity than in the optimum-size one. The spilled-over fuel from the cavity mixes with the annulus airflow and results in fuel-lean mixtures. As the local mixture becomes less fuel-lean with the reduced annulus flow, the temperature downstream of the forebody increases. Future calculations will be made for these flows employing a detailed-chemical-kinetics model for propane combustion to investigate the flame-stability characteristics in the trapped-vortex combustor.

Acknowledgment

This work was supported, in part, by U.S. Air Force Contract F33615-95-C-2507 and the U.S. Air Force Office of Scientific Research.

References

[1]Hsu, K.-Y., Goss, L. P., and Roquemore, W. M., "Characteristics of a Trapped-Vortex Combustor," *Journal of Propulsion and Power*, Vol. 14, No. 1, 1998, pp. 57–65.

[2]Rohsenow, W. M., Fink, C. H., and Pollis, S. R., "Flow Through Two Orifices in Series," American Society of Mechanical Engineers, Paper 51-A-87, 1951.

[3]Migay, V. K., "Study of Ribbed Diffusers," (in Russian), *Toploenergetika*, No. 10, 1962; English Translation, A.R.C. Paper 25, 1963, p. 382.

[4]Mair, W. A., "The Effect of a Rear-Mounted Disc on the Drag of a Blunt-Based Body of Revolution," *The Aeronautical Quarterly*, Vol. 10, Pt. 4, Nov. 1965, pp. 350–360.

[5]Roshko, A., and Koenig, K., "Interaction Effects on the Drag of Bluff Bodies in Tandem," Symposium on Aerodynamic Drag Mechanisms of Bluff Bodies and Road Vehicles, General Motors Research Lab., Sept. 1976.

[6]Little, B. H., and Whipkey, R. R., "Locked Vortex Afterbodies," *Journal of Aircraft*, Vol. 16, No. 5, 1979, pp. 296–302.

[7]Katta, V. R., and Roquemore, W. M., "Numerical Studies on Trapped-Vortex Concepts for Stable Combustion," *Journal of Engineering for Gas Turbines and Power* (to be published).

[8]Katta, V. R., and Roquemore, W. M., "Numerical Studies on Trapped-Vortex Combustor," AIAA Paper 96-2660, July 1996.

[9]Leonard, B. P., "A Stable and Accurate Convective Modeling Procedure Based on Quadratic Upstream Interpolation," *Computer Methods in Applied Mechanics and Engineering*, Vol. 19, 1979, p. 59.

[10]Katta, V. R., Goss, L. P., and Roquemore, W. M., "Numerical Investigations of Transitional H_2/N_2 Jet Diffusion Flames," *AIAA Journal*, Vol. 32, No. 1, 1994, pp. 84–94.

[11]Katta, V. R., Goss, L. P., and Roquemore, W. M., "Simulation of Vortical Structures in a Jet Diffusion Flame," *International Journal of Numerical Methods in Heat and Fluid Flow*, Vol. 4, 1994, pp. 413–424.

[12]Katta, V. R., and Roquemore, W. M., "Numerical Studies on the Structure of Two-Dimensional H_2/Air Premixed Jet Flame," *Combustion and Flame*, Vol. 102, Nos. 1 and 2, 1995, pp. 21–40.

[13]Durbin, M. D., Vangsness, D., Ballal, D., and Katta, V. R., "Study of Flame Stability in a Step Swirl Combustor," *Journal of Engineering for Gas Turbine and Power*, Vol. 118, No. 2, 1996, pp. 308–315.